Identification of hydrogeochemical and stable isotopic groundwater processes in the Laayoune-Dakhla region (Southern Sahara, Morocco)

Khalid Mizeb
University Ibn Tofail
Mohammad Ghalit (ghalit3@gmail.com)
Mostafa Doubi
University Ibn Tofail
Hamid Erramli
University Ibn Tofail
Mokhtar El Kanti
University Ibn Tofail

Research Article

Keywords: Groundwater, hydrogeochemical, mineralization, stable isotopic Laayoune-Dakhla

Posted Date: October 3rd, 2022

DOI: https://doi.org/10.21203/rs.3.rs-2110325/v1

Abstract

The assessment of major elements and stable isotopes of groundwater in the Laayoune-Dakhla region was carried out in order to determine the various geochemical processes that contribute to the mineralization of these waters. A total of 30 groundwater samples were collected from wells in the Laayoune-Dakhla region (southern Sahara, Morocco). Using a hydrogeochemical assessment technique, this study will look at the general conditions of groundwater for drinking reasons.

The statistical results of the major cations (Na^+, Ca^{2+}, Mg^{2+}, K^+) of the major anions (Cl^-, SO_4^{2-}, HCO_3^-, NO_3^-), show that the abundant cations and anions are of the order of $Na^+ > Ca^{2+} > Mg^{2+} > K^+$ and $Cl^- > SO_4^{2-} > HCO_3^- > NO_3^-$, respectively. The EC value of the water in the study area ranges from 1290 to 6895 µS/cm with an average of 3341.53 µS/cm. The pH value of the water samples is between 6.88 and 7.75. The waters of the study area were determined to be hydrogeochemical facies Na-Cl (86.66%) and Ca-SO_4 (13.33). Their chemistry seems to be mainly controlled by sulphate, calcium, chloride and sodium and is explained by the dissolution of the evaporative formations characteristic of the Saharan regions. Ionic reports show that rock weathering and mineral dissolution and evaporation control the chemical evolution of groundwater. In addition, a good correlation between calcium and sulphate suggests leaching of gypsum and anhydrite.

The values of $\delta^{18}O$ vary from − 6.96 to -8.93‰ while those of δ^2H vary between − 51.5 and − 65.56‰. The presence of evaporation was confirmed by stable isotope levels ($\delta^{18}O$, δ^2H). The variation in oxygene-18 levels can be interpreted in terms of the difference in altitude between the recharge altitudes.

Introduction

Groundwater is a precious and essential natural resource, flowing on the surface or in underground geological aquifers. Its chemical composition is related to the environment in which it is found, it is altered by the interaction between water and its environment (Liu et al. 2019a). Understanding hydrogeochemistry is essential for establishing the origin of groundwater's chemical composition and the interaction between water and rock (Richards et al. 2022).

Water quality is a factor that influences both human and animal health (Boelee et al. 2019). Natural processes (soil erosion, precipitation, evaporation) and human activity (agriculture, urban and industrial waste and waste water discharges) also impact its water quality (Es-sousy et al. 2018; Su et al. 2022). Therefore, understanding groundwater characteristics is critical for the management of groundwater resources in the study area (Zhang et al. 2020).

Different ionic ratios can be utilized to define water's chemical makeup, as some researchers have done to emphasize the development of groundwater chemistry (Lipiec et al. 2020; Romanova et al. 2021; Bouaissa et al. 2021).

Many studies have revealed that several geochemical processes, such as ion exchange, evaporation, rock weathering, and mineral dissolution, have an impact on groundwater chemistry (Liu et al. 2019b; Elmeknassi et al. 2022). Because the chemical makeup of water can limit its usage for various reasons such as drinking and agriculture, many researchers have looked into surface water/groundwater hydrochemistry to see if water consumption for the intended purpose is possible (Bouteldjaoui et al. 2020; Talabi et al. 2020; Mizeb et al. 2022).

In general, groundwater in deep aquifers retains its stable isotopic signature ($\delta^{18}O$, δ^2H) unless mixed with waters of different isotopic composition. Therefore, the determination of stable isotopic water composition can identify groundwater recharge from isotopically distinct water sources from meteoric waters (Jung et al. 2020), such as evaporated water, during vertical transfer to unconfined aquifers, or surface water bodies (Andries et al. 1988).

The ratio of freshwater δ^2H to $\delta^{18}O$ isotopes varies according to the spatial and temporal climatic regimes that govern the distribution of precipitation waters in geographic regions (Lone et al. 2022). The isotopic ratios (δ^2H/ $\delta^{18}O$), strongly dependent on temperature, it is a function of climatic hazards, altitude, latitude (McGill et al. 2021). It also depends on the amount of precipitation that plays a role in tropical and equatorial regions (Zhao et al. 2019).

Study Area

The Laayoune-Dakhla sedimentary basin (17°E – 11°E. 20°40'N – 28°48'N) in southern Morocco encompasses an area of about 326.810 km2. It is shown as tabular plains that run from north to south along the Atlantic Ocean, with widths ranging from 400 km to 400 m and heights ranging from 0 to 400 m. The basin is bounded on the west by the Atlantic Ocean and on the southeast by the Zemmour fault, which separates the older African massifs such as the Anti-Atlas chain, the Mauritani chain, and the Tindouf Basin. It has considerable groundwater resources that circulate in a complicated aquifer made up of shallow and deep aquifers (Fig. 1). Three aquifers are known in this basin: (1) Plio-Quaternary formations containing alluvial aquifers, such as the water layer of Laayoune and the Foum El Oued aquifer; (2) Paleogene aquifer containing marly sands; it's generally encountered at depths ranging from 150 to 300 m; and (3) Lower Cretaceous aquifer containing waters in sandstone It is the biggest in the Sahara basin due to its size and lithology, which allows for a massive supply of groundwater.

Geology

Morocco's Tarfaya-Aaiun (Laayoune) Basin extends from Tarfaya to Ifni along the Moroccan Sahara (Davison 2005). The regional geology especially in the Tarfaya basin has been discussed by several authors (Michard 1976; Martinis and Visintin 1966; Choubert et al. 1966). After a phase of emersion in the late Jurassic, in the North part of the basin, during the Neocomian a thick sequence of continental to marine deltaic (formation of Tan Tan) is deposited in the basin. The Tarfaya Basin is composed of Precambrian and Palezoic folded rocks which are discordantly covered by Mesozoic sediments whose thickness locally exceeds 12 km (Kolonic et al. 2002). The thickness of the Barremian formation, which has a sandy lagoon facies, ranges from 550 m to 1345 m (Edoulati et al. 2013). A sample NW-SE cross section (Fig. 2) from Gueltat Zemmour (SE) to Laâyoune (NW) reveals an embedding of normal sedimentary interfaces from East to West. Lower Cretaceous strata is beveled eastward towards Gueltat Zemmour, nearing Infra-Cambrian and Primary outcrops. The substratum is made up of basic quartzite (Edoulati et al. 2013). A Lower Cretaceous sequence of sands interbedded with clay was deposited on these basic strata (Edoulati et al. 2013).

The oil drilling reaches the ceiling of this sand at a depth of 625 m. The roof of white sand and red clay rises roughly and is just 117 m deep. (Edoulati et al. 2013). This rise in the roof of (1) Lower Cretaceous, (2) Triassic, and (3) Jurassic strata is caused by a normal fault or major flexure located in the north region of Sidi Khattari and even farther north between oil drilling (Michard 1976; Edoulati et al. 2013). The Lower Cretaceous gets deep and clayey in the west and towards the coast (Edoulati et al. 2013). The depth of the sand ceiling ranges from 625 meters in oil drilling to 850m in deep drilling in Boucraâ, and more than 1800m in the Boujdour area (Edoulati et al. 2013). The Oligocene (made of chalky clay-micrite and dolomitic sandstone clay) and Middle and Late Miocene (composed of red sandstone and plastic clays interbedded with sands) series that have evolved in this region (Edoulati et al. 2013).

In the basin's south, a consistent embedding sedimentary succession from SE to NW reflects Monocline structure (Fig. 3). A thick sequence of clastic Lower Cretaceous sands interbedded with clay, unconformably grounded on a Precambrian metamorphic substratum (Edoulati et al. 2013).

Claystone, marl, siltstone, and dolomitic limestone make up the Upper Albian to Lower Cenomanian sequence (Wiedmann et al. 1982). Deeper-water shale and limestone are found in the Upper Cenomanian-Turonian and Coniacian layers, followed by shallower-water oyster shell beds in the Santonian. All of the Palaeocene, Upper Cretaceous, and Lower Cretaceous are truncated by an erosional unconformity (Davison 2005). This erosion most likely occurred between the Santonian and Palaeocene epochs. Thin Eocene and Oligocene units are overlain by a thicker Miocene sequence that can exceed 1 km in thickness (Davison 2005).

Materials And Methods

Groundwater samples were collected from 30 wells (shallow and deep) in 2019. The locations of the wells are shown in Fig. 1. All samples were collected and stored in polyethylene bottles at 4°C. The analytical techniques adopted are those published by Rodier and Legube (2009). Physicochemical parameters such as temperature, pH and electrical conductivity were measured in situ. Concentrations of calcium, magnesium, sodium and potassium were analyzed by atomic absorption spectrophotometer

(iCE-3000 AAS. Thermo Scientific). Bicarbonates (HCO_3^-) and chlorides (Cl^-) by assay using hydrochloric acid and silver nitrate (0.1 N). Nitrates (NO_3^-) and sulfates (SO_4^{2-}) were determined by the colorimetric assay method using a UV-VIS spectrophotometer (CE-7500. Cecil).

Oxygen-18 ($\delta^{18}O$) and deuterium ($\delta^{2}H$) were determined by mass spectrometry. Using the methods proposed by EPSTEIN and MAYEDA (1953) and FRIEDMAN (1953), each sample was analysed three times to increase precision. The values are expressed in δ (‰) in relation to the international standard V-SMOW (Vienna-Standard Mean Ocean Water). The analytical uncertainties on the measurements are 0.1 for $\delta^{18}O$ and 1 for $\delta^{2}H$.

Furthermore, the figures are plotted by AquaChem 2014.2, which may display the relative quantities of various ions in each water sample visibly.

Results And Discussion

The results of the analyses of the physico-chemical parameters of the Laâyoune-Dakhla water are presented in Table 1.

Table 1
Results of the different physicochemical parameters

	T	pH	E.C	TDS	HCO_3^-	Cl^-	SO_4^{2-}	NO_3^-	Ca^{2+}	Mg^{2+}	Na^+	K^+
	°C		(µs/cm)	mg/L								
W1	36	7.48	4700	3210	201.37	1303.14	1190.79	0	422.44	129.28	913.85	30.11
W2	34.6	7.55	2880	2540	225.77	1175.00	1510.70	0	402.00	124.42	765.65	24.24
W3	54.5	7.32	6390	4740	152.55	684.19	1908.43	0	724.65	69.98	487.18	17.20
W4	40	7.33	3620	2470	189.16	959.63	744.24	0	349.50	61.24	618.44	20.72
W5	30	6.88	3030	2070	360.02	787.70	371.31	0	301.43	100.12	465.78	18.77
W6	30	7.00	2795	2120	360.02	816.41	381.40	0	333.47	40.34	448.76	19.94
W7	30	7.00	2584	1960	317.30	744.80	353.06	0	209.76	87.84	459.80	17.99
W8	29	6.90	6895	5230	353.92	2164.07	699.39	9.30	423.44	188.69	1310.43	17.20
W9	27	7.40	6750	5900	976.30	1074.14	2200.48	2.48	942.48	269.73	665.78	72.34
W10	29	6.93	1700	1400	475.96	400.94	165.55	0	134.07	59.29	307.84	10.17
W11	40	7.34	5600	4820	353.92	2327.29	239.21	6.82	322.24	128.18	1460.32	51.22
W12	22.1	7.22	4070	2780	139.74	709.71	1418.95	0	619.09	122.47	396.81	52.00
W13	49	7.45	3550	2420	128.14	808.97	600.44	0.62	221.24	39.85	637.97	13.69
W14	44	7.34	5010	4110	268.49	888.02	2378.69	0	733.56	48.60	691.46	19.16
W15	36	7.34	2630	1790	207.47	744.80	254.11	0	227.65	35.72	489.89	17.60
W16	33.5	7.75	2740	1870	164.75	798.33	249.30	0	157.11	30.25	574.75	19.16
W17	38.4	7.55	2307	1750	201.37	758.98	198.38	0	134.27	25.03	580.73	13.69
W18	28.3	7.21	2200	1500	256.28	572.87	266.11	0	224.45	47.63	359.79	8.99
W19	32	7.35	2210	1910	274.59	544.16	260.35	0	218.04	44.35	339.79	12.90
W20	36	7.42	2690	1830	183.06	629.59	717.29	0	343.08	52.49	439.80	18.11
W21	35	7.73	2175	1650	176.96	687.38	95.11	0	105.21	36.94	370.83	17.20
W22	35.5	7.29	2920	1990	170.86	758.98	220.00	0	150.30	37.91	505.67	12.90
W23	36.5	7.74	2780	1900	164.75	716.09	227.21	0.62	87.37	14.58	486.70	12.90
W24	32	7.75	5590	4820	109.84	1059.60	397.29	3.72	237.27	40.82	735.47	19.94
W25	36	7.14	2690	1840	231.88	687.38	199.35	14.88	142.48	36.94	465.55	9.78
W26	26	7.37	3320	2270	231.88	798.33	275.72	56.43	181.02	46.66	569.00	5.87
W27	24	7.38	2170	1480	183.06	487.08	180.13	54.57	129.08	30.13	296.80	5.08
W28	27.9	7.33	1610	1030	262.39	329.33	179.17	27.28	104.45	23.33	220.93	5.08
W29	26	7.44	1290	850	231.88	200.65	147.95	24.80	90.94	18.47	134.03	3.91
W30	26	7.33	1350	920	231.88	229.01	176.29	26.66	82.76	49.57	123.92	5.08

The pH values of soil water in the Laayoune-Dakhla region range from 6.88 to 7.75, with a mean value of 7.34 indicating the neutral nature of soil water in the study area.

High levels of E.C and TDS were found in soil water, with average values of 3341.53 S/cm for E.C and 850–5900 mg/L (averaging 2505.66 mg/L) for TDS. These values ranged from 1290 to 6895 S/cm for E.C.

Ca^{2+} and Mg^{2+} concentrations range from 82.76 to 942.48 mg/L and 14.58 to 269.73 mg/L, respectively, with mean values of 291.83 and 68.03 mg/L.

The study area's Na^{+} and K^{+} concentrations range from 123.92 to 1460.32 mg/L and 3.91 to 72.34 mg/L, respectively, with average values of 290.47 and 15.033 mg/L.

Major anion concentrations in the Laayoune-Dakhla region ranged from 200.65 to 2327.29 mg/L for Cl^{-}, 95.11 to 2378.69 mg/L for SO_4^{2-}, 109.84 to 976.30 mg/L for HCO_3^{-} and 0 to 56.43 mg/L for NO_3^{-}.

Nitrate levels (NO_3^{-}) in most samples are low, below the limit value defined by the Moroccan standard (50 mg/L) for most waters except for wells W26 and W27 with a maximum observed of 56.43 mg/L. Nitrate in groundwater owes its origin to activities such as the application of fertilizers on farms, the decomposition of plants, human wastewater, sumps and domestic effluents (El-Aziz 2017).

The Cl^{-} and SO_4^{2-} ions are the mass majority anions and the Na^{+} and Ca^{2+} are the mass majority cations. The mean molar abundance of the major elements (Table 1) varies as follows: for cations it is in descending order $Na^{+} > Ca^{2+} > Mg^{2+} > K^{+}$ and for anions it is in descending order $Cl^{-} > SO_4^{2-} > HCO_3^{-} > NO_3^{-}$.

Water hydrogeochemical

The word hydrochemical facies refers to the volumes of water that differ in their chemical makeup. The chemical nature of the groundwater studied is illustrated in the Piper diagrams (Fig. 5) the representation, focused on 30 water samples taken at the different sampling points during the monitoring of the physico-chemical quality of the waters of the Laayoune-Dakhla region

In the Piper diagram, we observe that: 86.66% of the water samples analyzed have dominant sodium chloride, while the remaining 13.33% of the samples show a dominance of calcium sulphate.

The facies of these water samples are sodium chlorides, probably due to the deposits of evaporites, with a slight tendency towards the sulphated calcium facies, these facies are probably due to the dissolution of the gypsum lens located in the marly formations of the Miocene or schist formations in the south of the Laâyoune-Dakhla region.

The quality of groundwater is influenced by many factors such as chemistry, geology of reservoir rocks and anthropogenic factors (Emenike et al. 2017; Ben-aazza et al. 2022).

Identification of hydrogeochemical processes

Water-rock interactions play an important role in changes in groundwater quality, which are also useful in determining the origin of groundwater. To elucidate the many hydrogeochemical mechanisms involved in the evolution of water chemistry, a correlation analysis between ionic elements was conducted using dispersion diagrams (Sangadi et al. 2022). When the correlation is very close to the right [1:1], it indicates that the degree of dependence is linear between the variables (Wu et al. 2019). This study may reveal the origin of the different waters and the processes that generated the chemical composition of the waters (Bouaissa et al. 2021; Iyakare et al. 2022).

To identify the hydrogeochemical processes that happened, many standard graphical displays are frequently used.

On the Na/Cl graph (Fig. 5), which is often used to identify processes responsible for the salinity of water (Najib et al. 2017), trend samples are located along the NaCl halite solubility line (i.e., where the Na/Cl molar ratio = 1) associated with marine spray carried by rainwater (sea salt), or the alteration of evaporites (Khan et al. 2021).

The results demonstrate that the correlation coefficient between the chemical components Na+ and Cl- in the samples is very high (R = 0.98) (Fig. 5). This demonstrates that the relationship between these two components is quite strong and that they are of the same origin.

It should be noted that the region has a dry environment with a high rate of evapotranspiration, which results in the creation of salt layers that are washed into groundwater (Bali et al. 2021).

Origin of Ca^{2+}, Mg^{2+}, HCO_3^- and SO_4^{2-} ions:

The graph of (SO_4^{2-} + HCO_3^-) as a function of (Ca^{2+} + Mg^{2+}) (Fig. 6) demonstrates that groundwater samples are distributed on line 1:1 (the least mineralized) and above. Samples close to 1:1 show that calcite, dolomite, and gypsum dissolution is the main process in the system (Hassen et al. 2016).

In a carbonated environment, the simultaneous enrichment of Ca^{2+} and the depletion of Mg^{2+} is mainly explained by the phenomenon of interaction between rock water such as dolomitization, dissolution and precipitation (Yu et al. 2020). A number of groundwater points studied show a ratio (Mg^{2+}/Ca^{2+}) different from the 1:1 line (Fig. 7), meaning that the concentration of calcium exceeds that of magnesium. It can be argued that the origin of calcium is mainly due to the dissolution of gypsum.

The dissolution of the dolomite should result in a 1:1 connection between alkalinity and (Ca^{2+} + Mg^{2+}). The association between alkalinity and (Ca^{2+} + Mg^{2+}) is weak (Fig. 8), showing that dolomite dissolution is not the main source of Ca^{2+} and Mg^{2+} in groundwater in the study region. The association between alkalinity and Ca^{2+} is quite weak (Fig. 8), indicating that the reduction in HCO_3^-.

Figure 9 shows that the majority of the samples are distributed around the gypsum dissolution line, confirming the origin of the solubility of the sulphate and calcium ions (Gypse). In addition, a good correlation between calcium and sulphate suggests leaching of gypsum and anhydrite when water flows underground.

The poor correlation between alkalinity and Na^+ (Fig. 10) further suggests that sodium carbonate dissolution is not substantial in the study area. In summary, hydrochemical facies are defined as evaporite (SO_4^{2-}) and halite dissolution.

As the search area is located in the arid zone (Sahara), which provides a favorable condition for evaporation and condensation. Due to evaporation, the Cl^- content of groundwater in arid areas is relatively higher, so it may reflect the degree of mineralization of groundwater. Figure 11 shows that the concentration of Cl^- increases with the increase in TDS, indicating that groundwater is definitely affected by evaporation.

Mineral dissolution/precipitation: Gibbs diagram

The reaction between groundwater and aquifer minerals plays an important role in water quality, which is also useful for understanding the origin of groundwater (Bozda and Göçmez 2013). Gibbs (Gibbs 1970) suggested a diagram in which the ratio of cations [(Na + K) / (Na + K + Ca)] and anions [Cl/ (Cl + HCO_3)] is expressed in relation to the TDS (Fig. 12).

Figure 12 clearly shows that the majority of the samples studied are in the evaporation zone where the effect of evaporation is dominant in the groundwater of the study area. Evaporative dissolution processes primarily control the chemistry of groundwater in this region.

It is noted that the majority of the samples are in the evaporation zone, which is probably related to climatic conditions (arid climate).

Saturation indices (SI) at chemical equilibrium

Recharge water quality and water interactions with soil and rocks during percolation and storage in aquifers are key determinants of groundwater chemistry (Keesari et al. 2020). Typically, saturation indices (SI) are used to express the tendency

of water to precipitation or dissolution of salts.

Based on the results of geochemical modelling during groundwater evolution, a significant relationship between SO_4^{2-} and S.I of the selected minerals was observed (Fig. 13). These results suggest that carbonate precipitation is strongly affected by the dissolution of evaporative minerals.

Isotope results

The stable isotopes of the water molecule are most commonly used in groundwater studies. They provide information on the origin of water and how groundwater is recharged, determine short- and long-term climatic variations, and allow quantitative assessment of the mixture and other processes such as evaporation (Gat 1980; Clark and Fritz 1997). The source of groundwater salinity can be determined using stable isotopes (Bahir et al. 2021). The stable isotopic compositions are comparable to that of the Craig-defined global meteoric water line (GMWL): $\delta^2H(‰) = 8*\delta^{18}O\ (‰) + 10$ (Craig 1961). This relationship was shown by Friedman (Friedman et al. 1964) to be the result of fractionation of the isotopic molecules of water during evaporation and condensation in the hydrological cycle.

Table 2 Results of isotopic analysis of samples collected from Laayoune-Dakhla

	T	pH	EC	TDS	Depth	^{18}O ‰	^{2}H ‰
W1	36	7.48	4700	3210	450	-8.78	-64.1
W2	34.6	7.55	2880	2540	629	-8.63	-62.55
W3	54.5	7.32	6390	4740	920	-8.93	-63.55
W4	40	7.33	3620	2470	650	-8.55	-63.05
W5	30	6.88	3030	2070	552	-8.78	-63.9
W6	30	7	2795	2120	452	-8.77	-65
W7	30	7	2584	1960	497	-8.76	-65.56
W8	29	6.9	6895	5230	450	-7.31	-57.64
W9	27	7.4	6750	5900	390	-8.82	-60.1
W10	29	6.93	1700	1400	260	-8.23	-58.13
W11	40	7.34	5600	4820	-	-	-
W12	22.1	7.22	4070	2780	145	-8.57	-63.6
W13	49	7.45	3550	2420	900	-8.32	-60.9
W14	44	7.34	5010	4110	881	-8.7	-63.25
W15	36	7.34	2630	1790	510	-8.32	-63.22
W16	33.5	7.75	2740	1870	470	-8.26	-63.31
W17	38.4	7.55	2307	1750	543	-8.37	-62.23
W18	28.3	7.21	2200	1500	315	-8.39	-62.67
W19	32	7.35	2210	1910	415	-8.42	-63.13
W20	36	7.42	2690	1830	490	-8.48	-62.36
W21	35	7.73	2175	1650	720	-8.65	-60.65
W22	35.5	7.29	2920	1990	525	-8.27	-63
W23	36.5	7.74	2780	1900	530	-8.43	-62.25
W24	32	7.75	5590	4820	350	-8.59	-62.65
W25	36	7.14	2690	1840	450	-6.96	-51.5
W26	26	7.37	3320	2270	180	-7.73	-58.25
W27	24	7.38	2170	1480	140	-8.4	-62.55
W28	27.9	7.33	1610	1030	175	-8.63	-62.75
W29	26	7.44	1290	850	156	-8.66	-62.85
W30	26	7.33	1350	920	165	-8.62	-63.45

The isotopic composition ($\delta^{2}H$, $\delta^{18}O$) is plotted on the diagram as a function of the local meteoric water line (LMWL) and the global meteoric water line (GMWL)(Fig. 14).

Evaporation typically occurs during surface runoff in lakes and reservoirs (Clark 2018). The influence of the isotopic exchange process that can alter the isotopic composition of groundwater should also be considered (Clark and Fritz 1997). The

atmospheric temperature is the most predominant factor controlling the isotopic composition and δD–$\delta^{18}O$ relationship of the waters (Li et al. 2020).

The isotopic values of oxygen and deuterium for the 30 groundwater samples collected in the study area (Table 2) range from – 6.96 to – 8.93 ‰ for $\delta^{18}O$ and – 51.5 to – 65.56 ‰ for $\delta^{2}H$. This range of variation characterizes an Atlantic origin of precipitation. These results are almost in the same order as those measured by Edoulati (2013). The regression results for $\delta^{18}O$ and $\delta^{2}H$ gave an equation defined by $\delta^{2}H = 5.35\ \delta^{18}O - 16.89$ (Fig. 14). Therefore, in a comparison of the values obtained at the two meteoric water lines, show that all points of the groundwater data are plotted to the right, defining a trend with a slope of 5.35 and reflecting an evaporation slope between 4 and 6 in semi-arid and arid areas (Clark and Fritz 1997; Abderamane et al. 2013; Ahmed et al. 2022). This suggests either evaporation of raindrops before reaching the ground (Sun et al. 2020), or delayed infiltration of precipitation, and a mixture of meteoric water with evaporated precipitation water in a few samples (Edoulati et al. 2013).

Determining the altitudes and recharge zones of the sources is essential for estimating groundwater resources. Stable isotope levels can be used to determine recharge elevations; the isotopic signal of seepage water is often a function of the temperature of the soil where the seepage occurs (Tazioli et al. 2019).

We sought to determine the possible relationship between the isotopic ratio of $\delta^{18}O$ and the altitude of water infiltration. Figure 15 shows the values of $\delta^{18}O$ and the altitudes of the different groundwater.

In Figure 15 we have drawn the line giving the regional altitude isotopic gradient estimated at -0.52‰ per 100 m. The values obtained are different from those given in the bibliography. On a Morocco scale, the regional altitude isotopic gradient is -0.27‰ per 100 m of elevation (Miche et al. 2018). The water be recharged at altitudes not to rise (not to exceed 300 m).

Differences in isotopic compositions between the aquifer and precipitation (which have been used to determine the gradient) cannot be attributed to an altitude impact. However, this exhaustion may be due to the temperature of the soil.

Conclusion

The combined hydrochemical and stable isotopic ($\delta^{18}O$, $\delta^{2}H$) approach applied in this study has led to a better understanding of the functioning of the groundwater system in the Laayoune-Dakhla region, the mineralization processes that underlie significant variations in composition. The hydrochemical data revealed that the abundant cations and anions are of the order of $Na^{+} > Ca^{2+} > Mg^{2+} > K^{+}$ and $Cl^{-} > SO_4^{2-} > HCO_3^{-} > NO_3^{-}$ respectively. Two dominant hydrochemical facies are observed in the groundwater of the study area: Na-Cl and Ca-SO_4, with Na-Cl abundance (86.66%).

The main processes controlling the mineralization of the waters are the evaporation phenomenon and the dissolution of the minerals. Stable isotope data showed a significant source of recharge of meteoric waters related to a predominance of evaporation in the increase in salt concentration. The waters shall be recharged at altitudes not exceeding 300 m.

Declarations

Compliance with ethical standards

Conflict of interest The authors declare that they have no conflict of interest.

Ethical approval This article does not contain any studies with human participants or animals performed by any of the authors.

Funding declaration This research received no specific grant from any funding agency in the public, commercial, or not-for-profit sectors.

Data availability statement No datasets were generated or analyzed during the current study.

Author Contributions Statement

K. Mizeb: wrote the main manuscript text

M. Ghalit: wrote the main manuscript text and prepared figures

M. Doubi: wrote the main manuscript text

H. Erramli: wrote the main manuscript text

All authors reviewed the manuscript.

References

1. Abderamane H, Razack M, Vassolo S (2013) Hydrogeochemical and isotopic characterization of the groundwater in the Chari-Baguirmi depression, Republic of Chad. Environmental earth sciences, 69(7), 2337-2350. https://doi.org/10.1007/s12665-012-2063-7
2. Ahmed M, Chen Y, & Khalil M M (2022) Isotopic composition of groundwater resources in arid environments. Journal of Hydrology, 609, 127773. https://doi.org/10.1016/j.jhydrol.2022.127773
3. Andries C W, Kanyerere T, Israel S, & Butler M (2021) The application of environmental isotopes to conceptualize groundwater recharge in a coastal aquifer system: Case study of the West Coast Aquifer System, South Africa. Physics and Chemistry of the Earth, Parts A/B/C, 124, 102995. https://doi.org/10.1016/j.pce.2021.102995
4. Bahir M, Ouhamdouch S, & Ouazar D (2021) An assessment of the changes in the behavior of the groundwater resources in arid environment with global warming in Morocco. Groundwater for Sustainable Development, 12, 100541. https://doi.org/10.1016/j.gsd.2020.100541
5. Bali K M, Eltarabily M G, Berndtsson R, & Selim T (2021) Nutrient and salinity management for spinach production under sprinkler irrigation in the low desert region of California. Irrigation Science, 39(6), 735-749. https://doi.org/10.1007/s00271-021-00740-4
6. Boelee E, Geerling G, van der Zaan B, Blauw A, & Vethaak A D (2019) Water and health: From environmental pressures to integrated responses. Acta tropica, 193, 217-226. https://doi.org/10.1016/j.actatropica.2019.03.011
7. Bouaissa M, Gharibi E, Ghalit M, Taupin J D, & El Khattabi J (2021) Identifying the origin of groundwater salinization in the Bokoya massif (central Rif, northern Morocco) using hydrogeochemical and isotopic tools. Groundwater for Sustainable Development, 14, 100646. https://doi.org/10.1016/j.gsd.2021.100646
8. Bouteldjaoui F, Bessenasse M, Taupin J D, Kettab A (2020) Mineralization mechanisms of groundwater in a semi-arid area in Algeria: statistical and hydrogeochemical approaches. Journal of Water Supply: Research and Technology-AQUA, IWA publishing. https://doi.org/10.2166/aqua.2019.116
9. Bozdağ A, & Göçmez G (2013) Evaluation of groundwater quality in the Cihanbeyli basin, Konya, Central Anatolia, Turkey. Environmental earth sciences, 69(3), 921-937. https://doi.org/10.1007/s12665-012-1977-4
10. CHOUBERT G, FAURE-MURET A, & HOTTINGER L (1966) Aperçu géologique du Basin Côtier de Tarfaya. Notes et Mém. Serv. Geól. Maroc, 175 (I), 7-106, Rabat.
11. Clark I, Fritz P (1997) Environmental isotopes in hydrology. Lewis Publishers, Boca Raton
12. Clark I D, & Jautzy J J (2018) Environmental Isotope Tracers. State of the Science and Practice, 15.
13. Craig H (1961) Isotopic variations in meteoric waters. Science, 133(3465), 1702-1703.
14. Davison I (2005) Central Atlantic margin basins of North West Africa: geology and hydrocarbon potential (Morocco to Guinea). Journal of African Earth Sciences, 43(1-3), 254-274. https://doi.org/10.1016/j.jafrearsci.2005.07.018
15. Edoulati N, Boutaleb S, Bettar I, & Ouchbani A (2013) Contributions of chemical and isotopictools for understanding the groundwater modes recharge and flow in the lower Cretaceous aquifer in the Moroccan Sahara. DOI:10.4236/jwarp.2013.52020

16. El-Aziz S H A (2017) Evaluation of groundwater quality for drinking and irrigation purposes in the north-western area of Libya (Aligeelat). Environmental earth sciences, 76(4), 147. https://doi.org/10.1007/s12665-017-6421-3
17. Elmeknassi M, Bouchaou L, El Mandour A, Elgettafı M, Himi M, & Casas A (2022) Multiple stable isotopes and geochemical approaches to elucidate groundwater salinity and contamination in the critical coastal zone: A case from the Bou-areg and Gareb aquifers (North-Eastern Morocco). Environmental Pollution, 300, 118942. https://doi.org/10.1016/j.envpol.2022.118942
18. Emenike C P, Tenebe I T, Omole D O, Ngene B U, Oniemayin B I, Maxwell O, & Onoka B I (2017) Accessing safe drinking water in sub-Saharan Africa: Issues and challenges in South–West Nigeria. Sustainable cities and society, 30, 263-272. https://doi.org/10.1016/j.scs.2017.01.005
19. Epstein S, & Mayeda T (1953) Variation of O18 content of waters from natural sources. Geochimica et cosmochimica acta, 4(5), 213-224. https://doi.org/10.1016/0016-7037(53)90051-9
20. Es-sousy M, Gharibi E, Ghalit M, Taupin J D, & Ben Alaya M (2018, November) Hydrochemical quality of the Angads plain groundwater (Eastern Morocco). In Conference of the Arabian Journal of Geosciences (pp. 99-102). Springer, Cham. https://doi.org/10.1007/978-3-030-01572-5_24
21. Ben-aazza S, Hadfı A, Mohareb S, Karmal I, Hafid N, & Driouiche A (2020) Geochemical characterization and thermodynamic study of water scaling phenomenon at Tiznit region in Southern Morocco. Groundwater for sustainable development, 11, 100379. https://doi.org/10.1016/j.gsd.2020.100379
22. Friedman I (1953) Deuterium content of natural waters and other substances. Geochimica et cosmochimica acta, 4(1-2), 89-103. https://doi.org/10.1016/0016-7037(53)90066-0
23. Friedman I, Redfield AC, Schoen B, Harris J (1964) The variation of the deuterium content of natural waters in the hydrological cycle. Rev Geophys 2:177–224. https://doi.org/10.1029/RG002i001p00177
24. Gat J R (1980) The isotopes of hydrogen and oxygen in precipitation. In Handbook of environmental isotope geochemistry. Vol. 1.
25. Gibbs R J (1970) Mechanisms controlling world water chemistry. Science, 170(3962), 1088-1090.
26. Iyakare J D, Taupin J D, Hitimana C N, Dusabimana T, Ghalit M, El Ouahabi M, ... & Gharibi E K (2022) Hydrochemical study of bottled water in Rwanda and relationship with their origin. Water Supply, 22(1), 1155-1167. https://doi.org/10.2166/ws.2021.211
27. Jung H, Koh D C, Kim Y S, Jeen S W, & Lee J (2020) Stable isotopes of water and nitrate for the identification of groundwater flowpaths: A review. Water, 12(1), 138. https://doi.org/10.3390/w12010138
28. Keesari T, Roy A, Mohokar H, Pant D, & Sinha U K (2020) Characterization of mechanisms and processes controlling groundwater recharge and its quality in drought-prone region of Central India (Buldhana, Maharashtra) using isotope hydrochemical and end-member mixing modeling. Natural Resources Research, 29(3), 1951-1973. https://doi.org/10.1007/s11053-019-09550-0
29. Khan F, Krishnaraj S, Raja P, Selvaraj G, & Cheelil R (2021) Impact of hydrogeochemical processes and its evolution in controlling groundwater chemistry along the east coast of Tamil Nadu and Puducherry, India. Environmental Science and Pollution Research, 28(15), 18567-18588. https://doi.org/10.1007/s11356-020-10912-y
30. Kolonic S, Sinninghe Damste J S, Bottcher M E, Kuypers M M M, Kuhnt W, Beckmann B, … Wagner T (2002) geochemical characterization of cenomanian/turonian black shales from the tarfaya basin (sw Morocco). relationships between palaeoenvironmental conditions and early sulphurization of sedimentary organic matter1. Journal of Petroleum Geology, 25(3), 325–350. https://doi.org/10.1111/j.1747-5457.2002.tb00012.x
31. Li Y, An W, Pang H, Wu S Y, Tang Y, Zhang W, & Hou S (2020) Variations of stable isotopic composition in atmospheric water vapor and their controlling factors—A 6-year continuous sampling study in Nanjing, Eastern China. Journal of Geophysical Research: Atmospheres, 125(22), e2019JD031697. https://doi.org/10.1029/2019JD031697
32. Lipiec I, Wątor K, & Kmiecik E (2020) The application of selected hydrochemical indicators in the interpretation of hydrogeochemical data–A case study from Busko-Zdrój and Solec-Zdrój (Poland). Ecological Indicators, 117, 106460. https://doi.org/10.1016/j.ecolind.2020.106460

33. Liu J, Gao Z, Wang M, Li Y, Shi M, Zhang H, & Ma Y (2019a) Hydrochemical characteristics and possible controls in the groundwater of the Yarlung Zangbo River Valley, China. Environmental Earth Sciences, 78(3), 1-11. https://doi.org/10.1007/s12665-019-8101-y
34. Liu M, Xiao C, & Liang X (2019b) The hydrochemical characteristics and quality assessment of groundwater in Shuangliao City, China. In E3S Web of Conferences (Vol. 98, p. 01034). EDP Sciences. https://doi.org/10.1051/e3sconf/20199801034
35. Lone S A, Jeelani G, Padhya V, & Deshpande R D (2022) Identifying and estimating the sources of river flow in the cold arid desert environment of Upper Indus River Basin (UIRB), western Himalayas. Science of The Total Environment, 832, 154964. https://doi.org/10.1016/j.scitotenv.2022.154964
36. Martinis B, & Visintin V (1966) Données géologiques sur le bassin sédimentaire côtier de Tarfaya (Maroc méridional). Bassins sédimentaires du littoral africain, 13-26.
37. McGill L M, Brooks J R, & Steel E A (2021) Spatiotemporal dynamics of water sources in a mountain river basin inferred through δ2H and δ18O of water. Hydrological processes, 35(3), e14063. https://doi.org/10.1002/hyp.14063
38. Michard A (1976) Eléments de Géologie marocaine.
39. Miche, H., Saracco, G., Mayer, A., Qarqori, K., Rouai, M., Dekayir, A., ... & Emblanch, C. (2018). Hydrochemical constraints between the karst Tabular Middle Atlas Causses and the Saïs basin (Morocco): implications of groundwater circulation. Hydrogeology Journal, 26(1), 71-87. https://doi.org/10.1007/s10040-017-1675-0
40. Mizeb K, Doubi M, Ghalit M, El Kanti M, HACHI T, Abba E H, & Erramli H (2022) Quality assessment of groundwater in the region of Laayoune-Dakhla (southern Sahara Morocco) for drinking and irrigation purposes. Moroccan Journal of Chemistry, 10(3), 10-3. https://doi.org/10.48317/IMIST.PRSM/morjchem-v10i3.33070
41. Najib S, Fadili A, Mehdi K, Riss J, & Makan A (2017) Contribution of hydrochemical and geoelectrical approaches to investigate salinization process and seawater intrusion in the coastal aquifers of Chaouia, Morocco. Journal of contaminant hydrology, 198, 24-36. https://doi.org/10.1016/j.jconhyd.2017.01.003
42. Ouda B, El Hamdaoui A, & Ibn Majah M (2005) Isotopic composition of precipitation at three Moroccan stations influenced by oceanic and Mediterranean air masses. Isotopic composition of precipitation in the Mediterranean Basin in relation to air circulation patterns and climate, 125-140.
43. Richards L A, Fox B G, Bowes M J, Khamis K, Kumar A, Kumari R, ... & Polya D A (2022) A systematic approach to understand hydrogeochemical dynamics in large river systems: Development and application to the River Ganges (Ganga) in India. Water Research, 211, 118054. https://doi.org/10.1016/j.watres.2022.118054
44. Rodier J, Legube B, Merlet N, Brunet R (2009) L'analyse de l'eau [water analysis]. Dunod, Paris.
45. Romanova A, Porowski A, Zielski T, & Dancewicz A (2021) Origin and evolution of chemical composition of mineral waters of Szczawno-Zdrój inferred from long-term variation of ionic ratios, Sudetes Mts.(SW Poland). Environmental Earth Sciences, 80(10), 1-17. https://doi.org/10.1007/s12665-021-09643-1
46. Sangadi P, Kuppan C, & Ravinathan P (2022) Effect of hydro-geochemical processes and saltwater intrusion on groundwater quality and irrigational suitability assessed by geo-statistical techniques in coastal region of eastern Andhra Pradesh, India. Marine Pollution Bulletin, 175, 113390. https://doi.org/10.1016/j.marpolbul.2022.113390
47. Su F, Li P, & Fida M (2022) Dominant factors influencing changes in the water quantity and quality in the Dianshi Reservoir, East China. Human and Ecological Risk Assessment: An International Journal, 28(3-4), 387-407. https://doi.org/10.1080/10807039.2022.2053355
48. Sun C, Chen W, Chen Y, & Cai Z (2020) Stable isotopes of atmospheric precipitation and its environmental drivers in the Eastern Chinese Loess Plateau, China. Journal of Hydrology, 581, 124404. https://doi.org/10.1016/j.jhydrol.2019.124404
49. Talabi AO, Abdu-Raheem YA, Afolagboye LO, Oguntuase MA, Akinola OO (2020) Hydrogeochemistry of shallow groundwater in ado-Ekiti area. Southwestern Nigeria Groundwater for Sustainable Development 11: 100386. https://doi.org/10.1016/j.gsd.2020.100386
50. Tazioli A, Cervi F, Doveri M, Mussi M, Deiana M, & Ronchetti F (2019) Estimating the isotopic altitude gradient for hydrogeological studies in mountainous areas: Are the low-yield springs suitable? Insights from the northern Apennines of Italy. Water, 11(9), 1764. https://doi.org/10.3390/w11091764

51. Wiedmann J, Butt A, & Einsele G (1982) Cretaceous stratigraphy, environment, and subsidence history at the Moroccan continental margin. In Geology of the northwest African continental margin (pp. 366-395). Springer, Berlin, Heidelberg. https://doi.org/10.1007/978-3-642-68409-8_15
52. Wu J, Li P, Wang D, Ren X, & Wei M (2019) Statistical and multivariate statistical techniques to trace the sources and affecting factors of groundwater pollution in a rapidly growing city on the Chinese Loess Plateau. Human and Ecological Risk Assessment: An International Journal. https://doi.org/10.1080/10807039.2019.1594156
53. Yu Y, Song X, Zhang Y, & Zheng F (2020) Assessment of water quality using chemometrics and multivariate statistics: a case study in chaobai river replenished by reclaimed water, North China. Water, 12(9), 2551. https://doi.org/10.3390/w12092551.
54. Zhang B, Zhao D, Zhou P, Qu S, Liao F, & Wang G (2020) Hydrochemical characteristics of groundwater and dominant water–rock interactions in the Delingha Area, Qaidam Basin, Northwest China. Water, 12(3), 836. https://doi.org/10.3390/w12030836
55. Zhao P, Guo Z S, She D L, & Tang X Y (2019) Spatial distribution of the oxygen-18 in precipitation in China based on a new empirical model. Journal of Mountain Science, 16(11), 2605-2614. https://doi.org/10.1007/s11629-019-5514-8

Figures

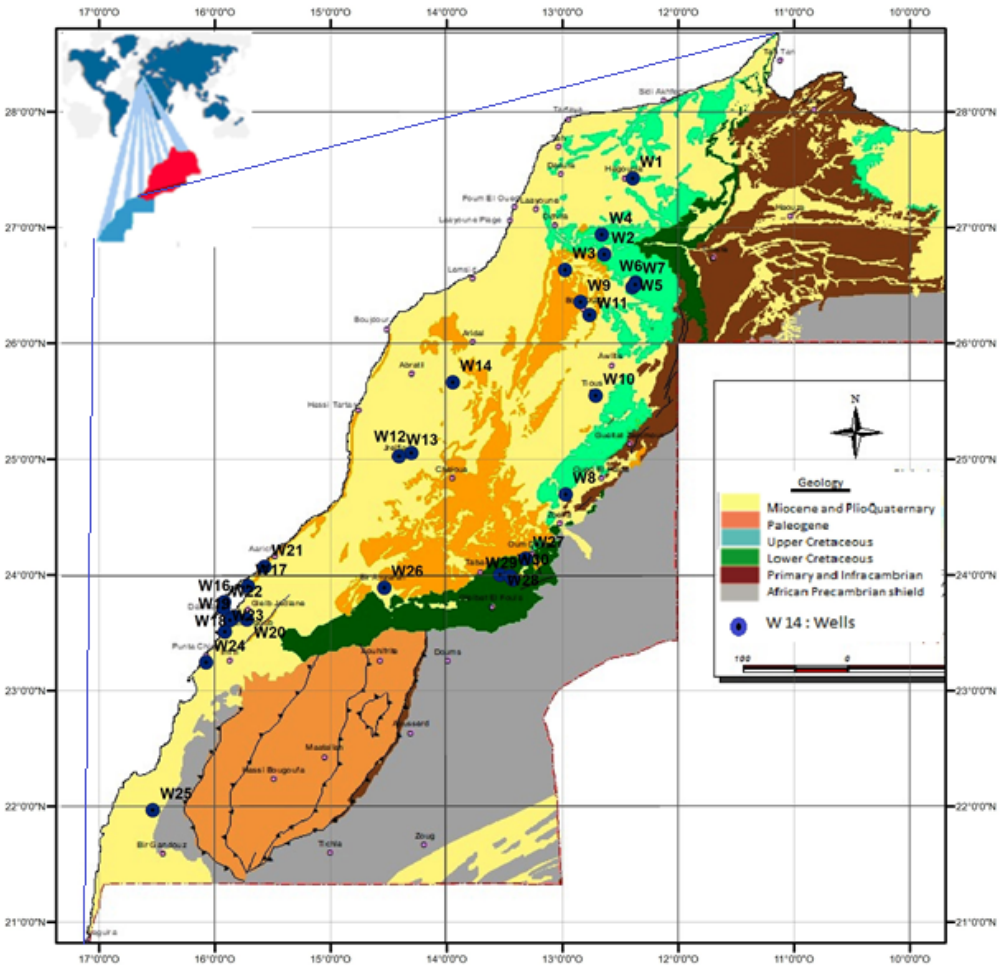

Figure 1

Geographical situation of Laayoune-Dakhla, exhibiting the roof of Lower Cretaceous rocks and the structural Basin (Mizeb et al. 2022)

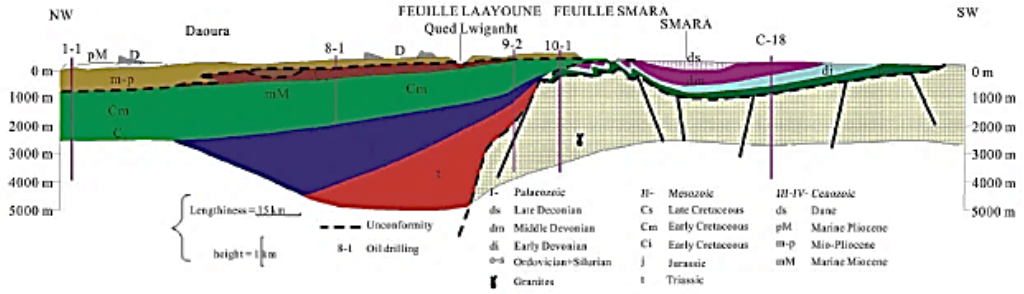

Figure 2

Schematic geological cross sections according to geophysics and drilling in the Laayoune-Dakhla Plain (Edoulati et al. 2013).

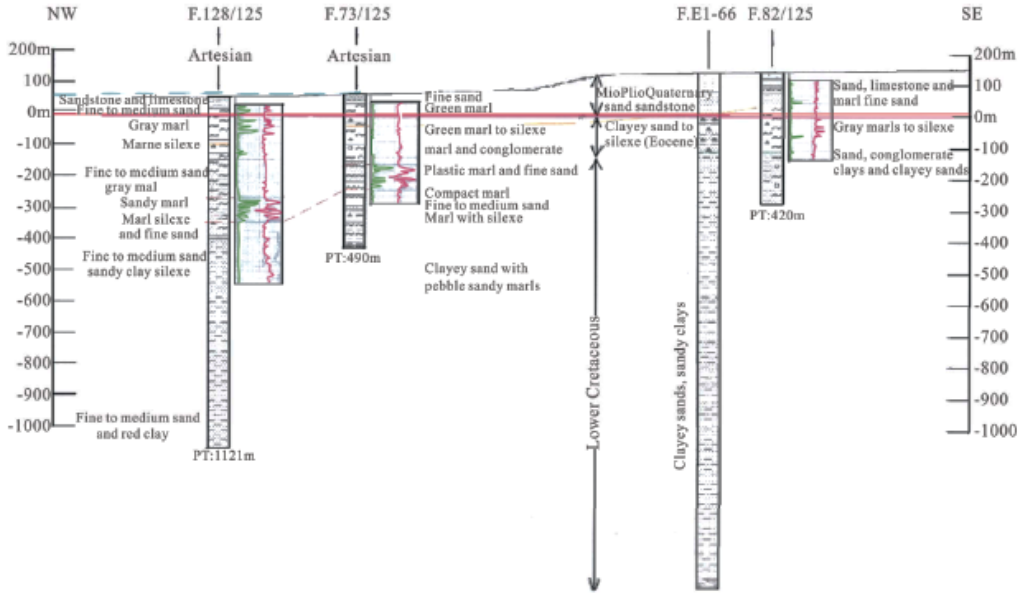

Figure 3

Logs of deep oil and hydrogeologic boreholes showing the stratigraphy of thesubsurface of Laayoune-Dakhla plain (Edoulati et al. 2013).

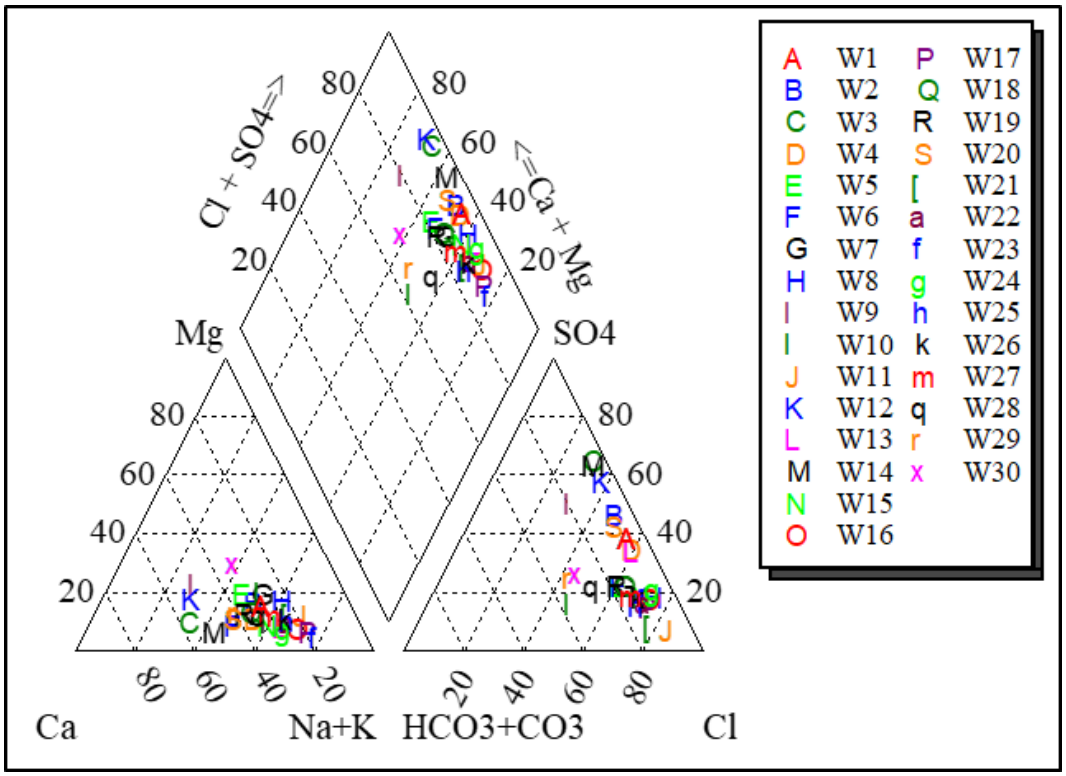

Figure 4

Piper diagrams representing all water categories of study area

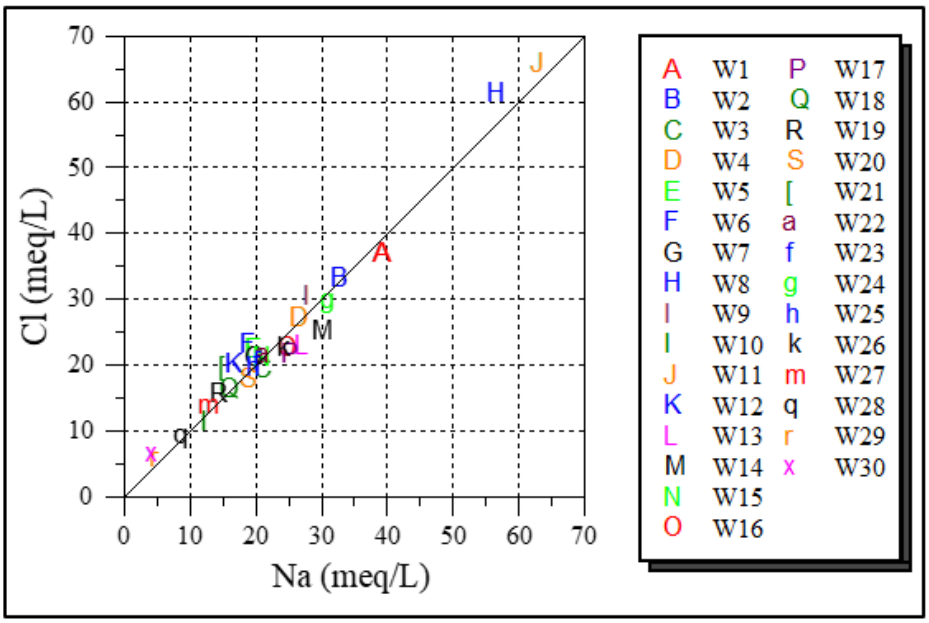

Figure 5

Diagram of the chloride concentration as a function of the sodium concentration of the samples.

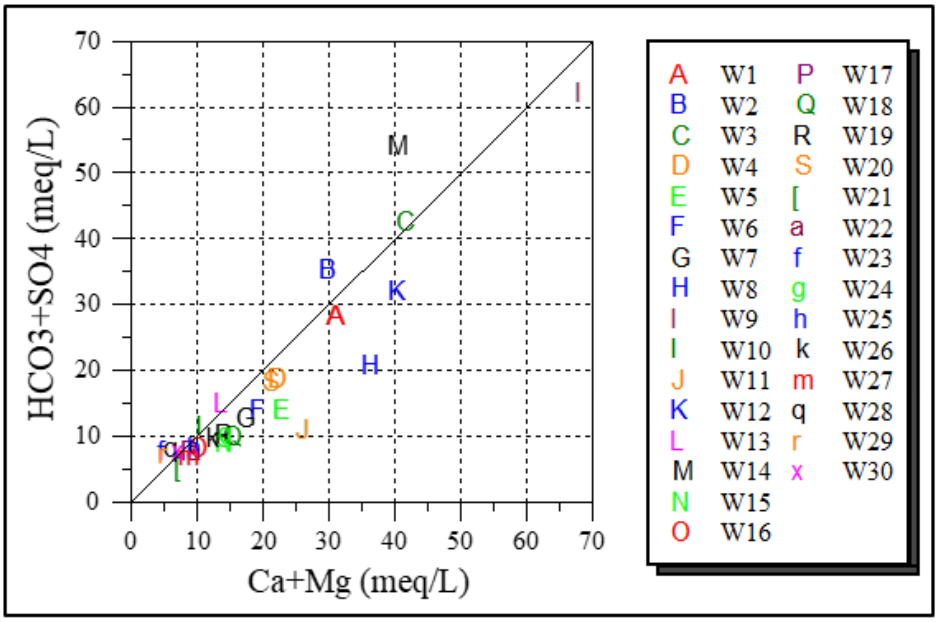

Figure 6

The graphic representation of (Ca^{2+} + Mg^{2+}) as a function of (SO_4^{2-} + HCO_3^-).

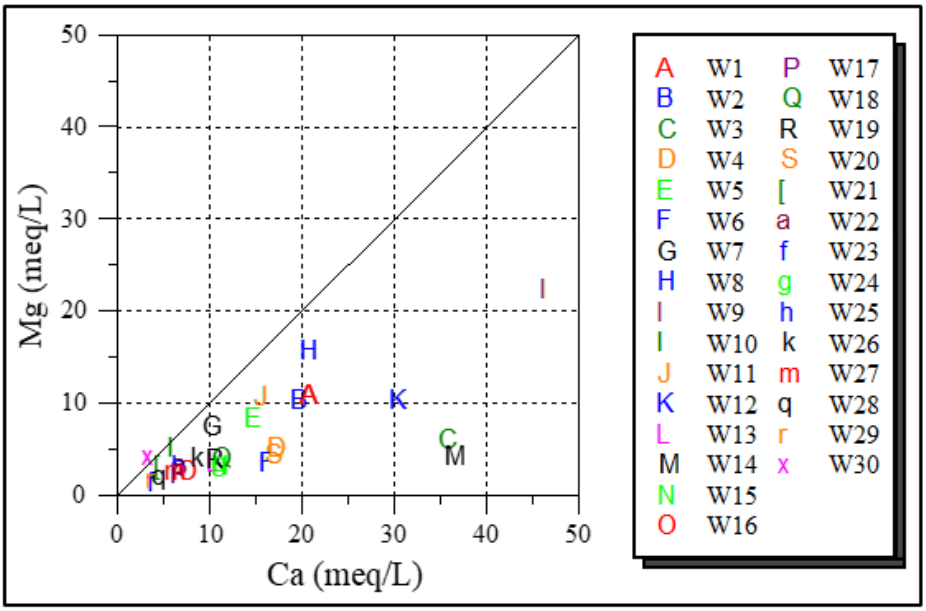

Figure 7

The graphic representation of Ca^{2+} as a function of Mg^{2+}.

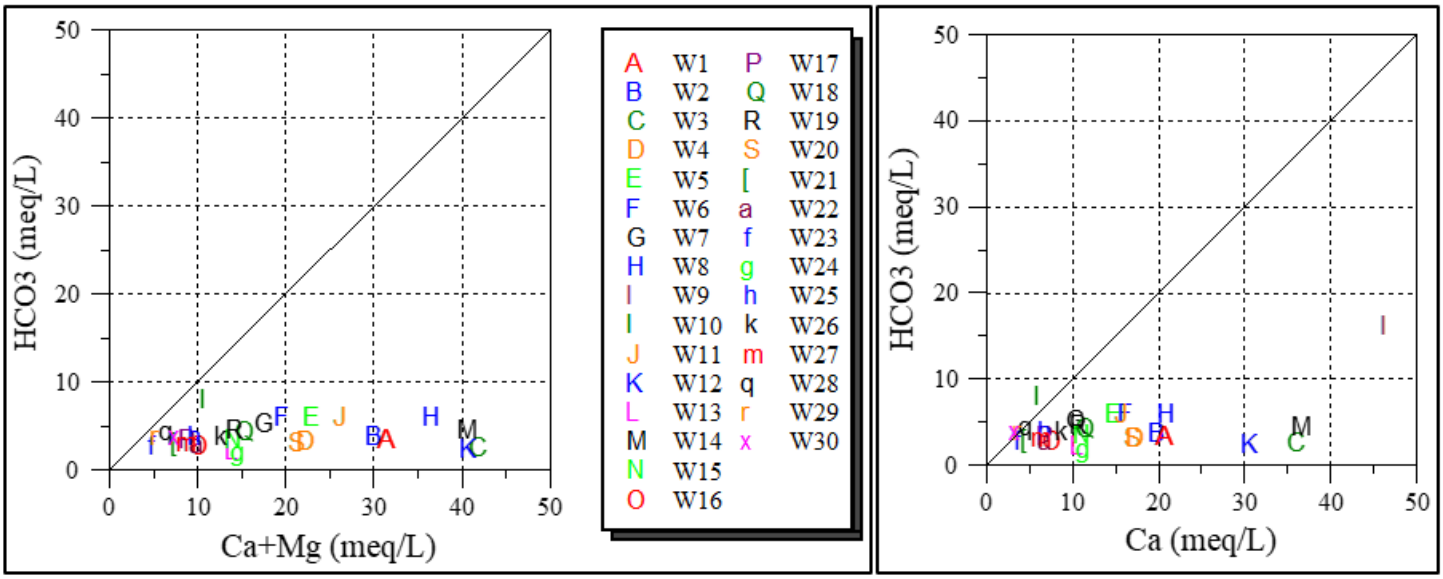

Figure 8

The graphical representation of Ca^{2+} + Mg^{2+} versus HCO^{3-} and Ca^{2+} versus HCO^{3-}.

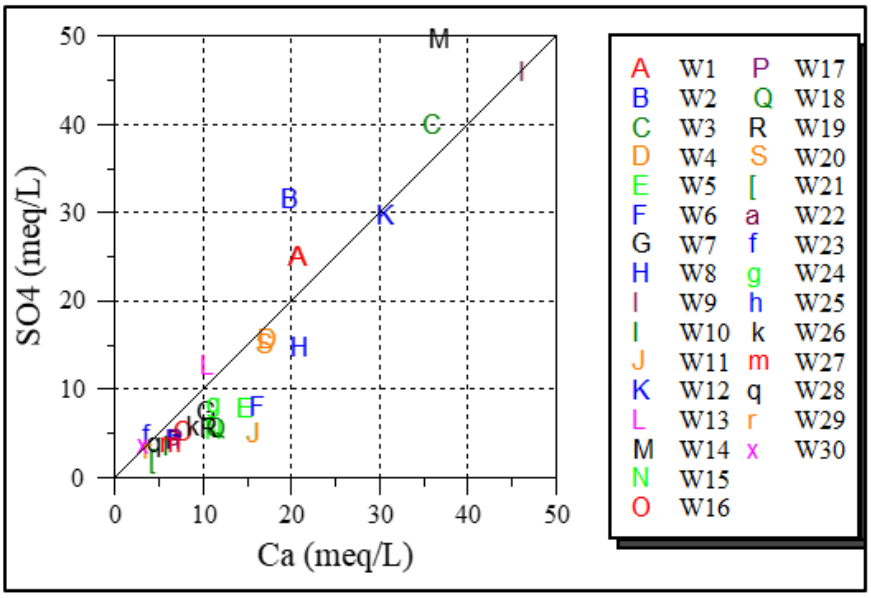

Figure 9

The graphic representation of Ca^{2+} as a function of SO_4^{2-}

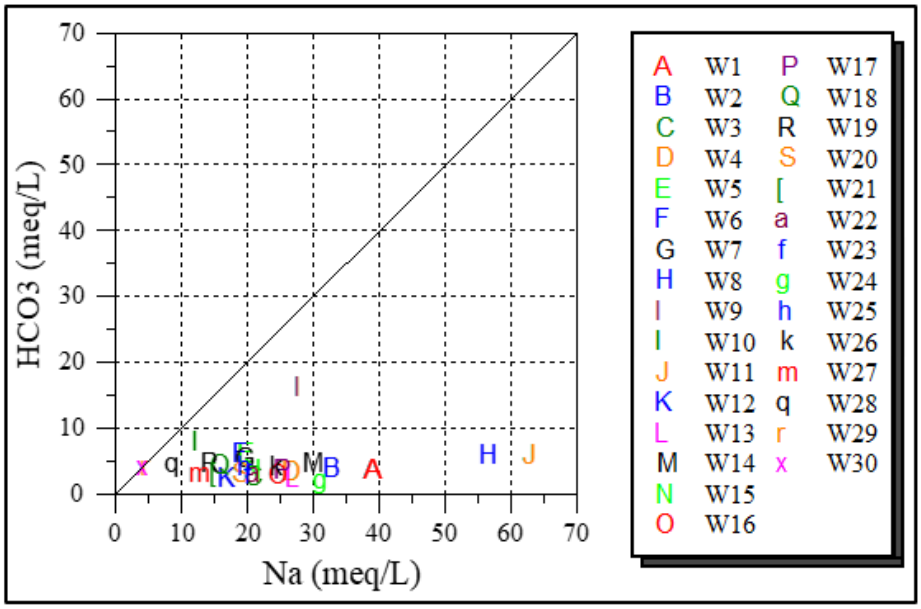

Figure 10

The graphic representation of Na^+ as a function of HCO_3^-

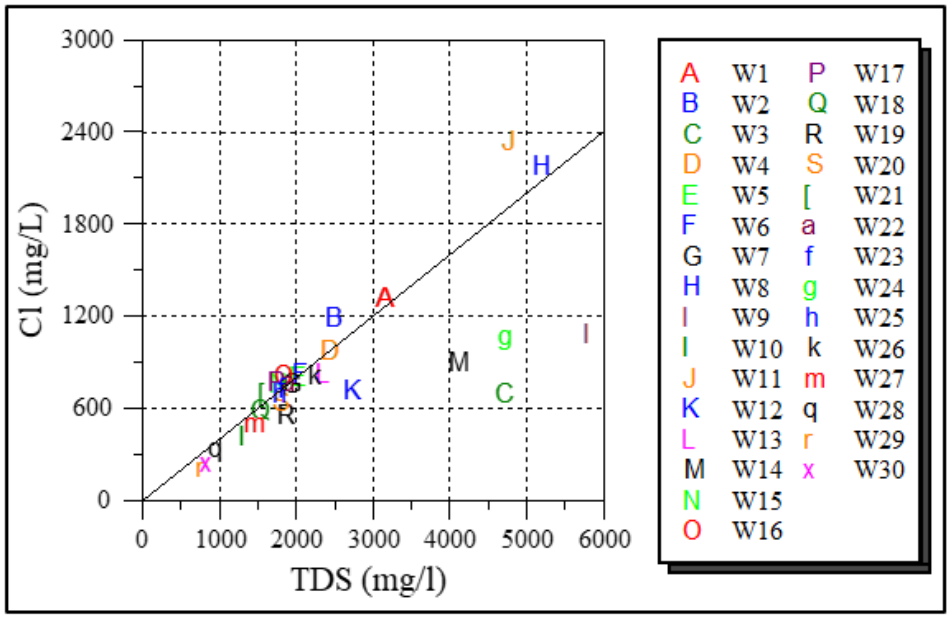

Figure 11

The graphic representation of TDS as a function of Cl-

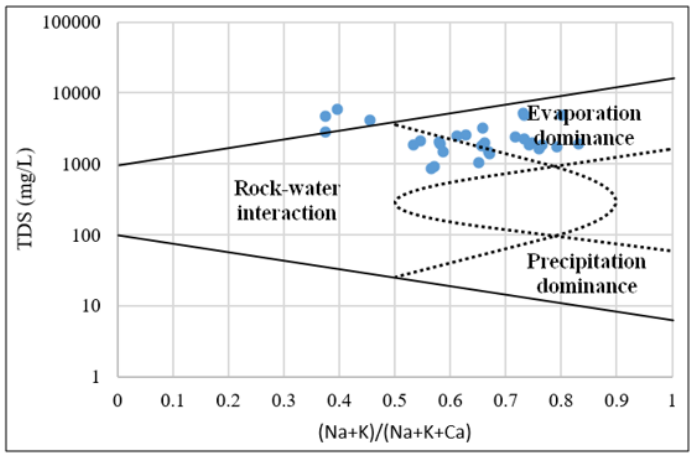

a) Gibbs diagram for cations

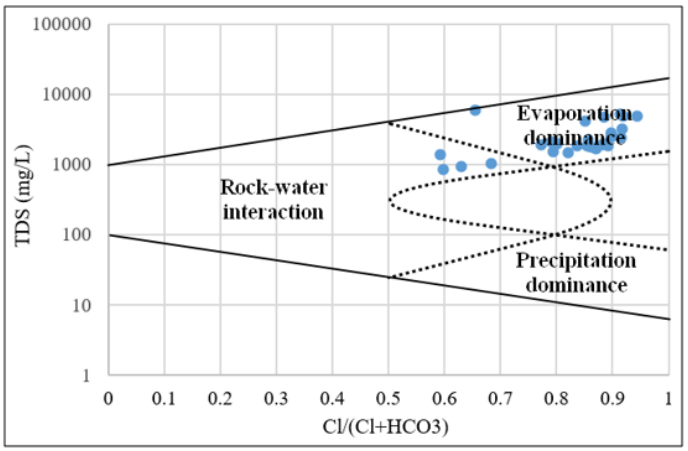

b) Gibbs diagram for anions.

Figure 12

Gibbs diagram for groundwater samples from the Laayoune-Dakhla region

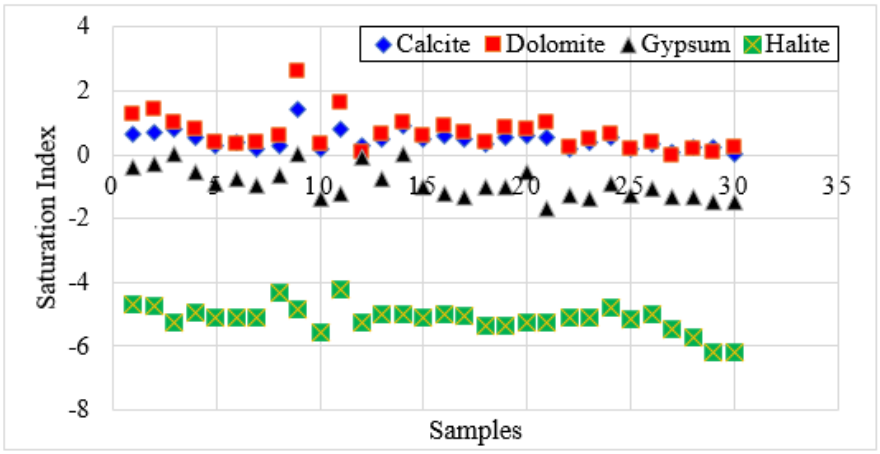

Figure 13

Evolution of the mineral saturation index according to the samples.

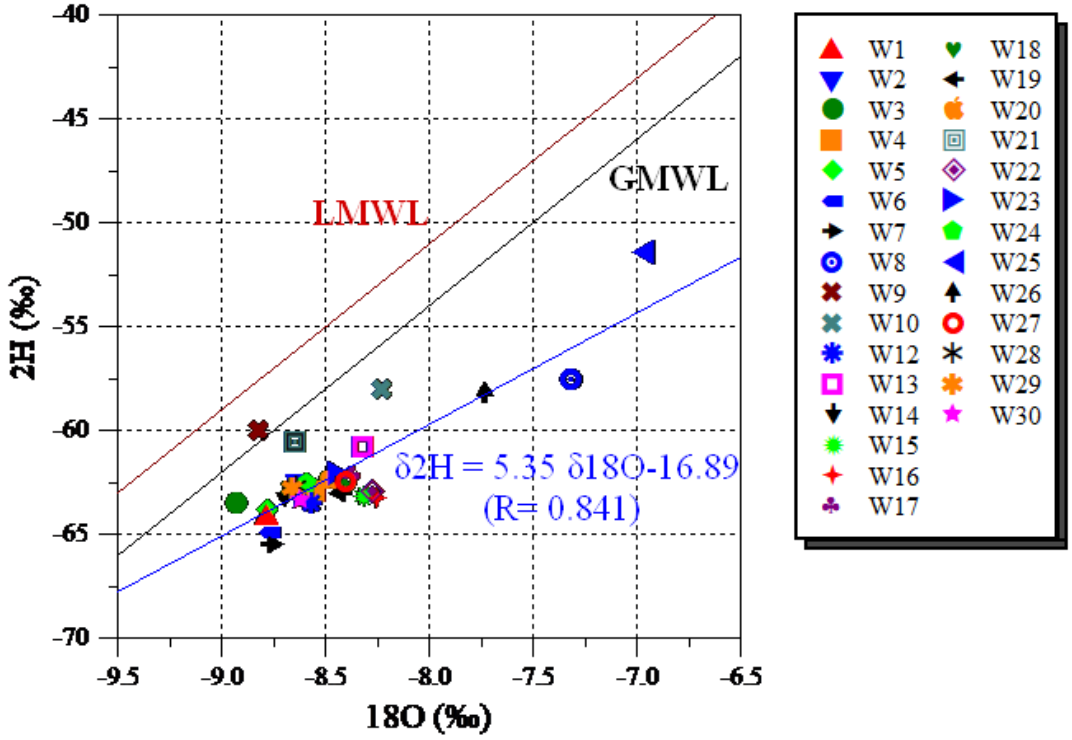

Figure 14

Relationship of $d^{2}H$ to $d^{18}O$ of groundwater to the local meteoric water line (LMWL) (Ouda et al. 2005) and the global meteoric water line (Craig 1961) (GMWL).

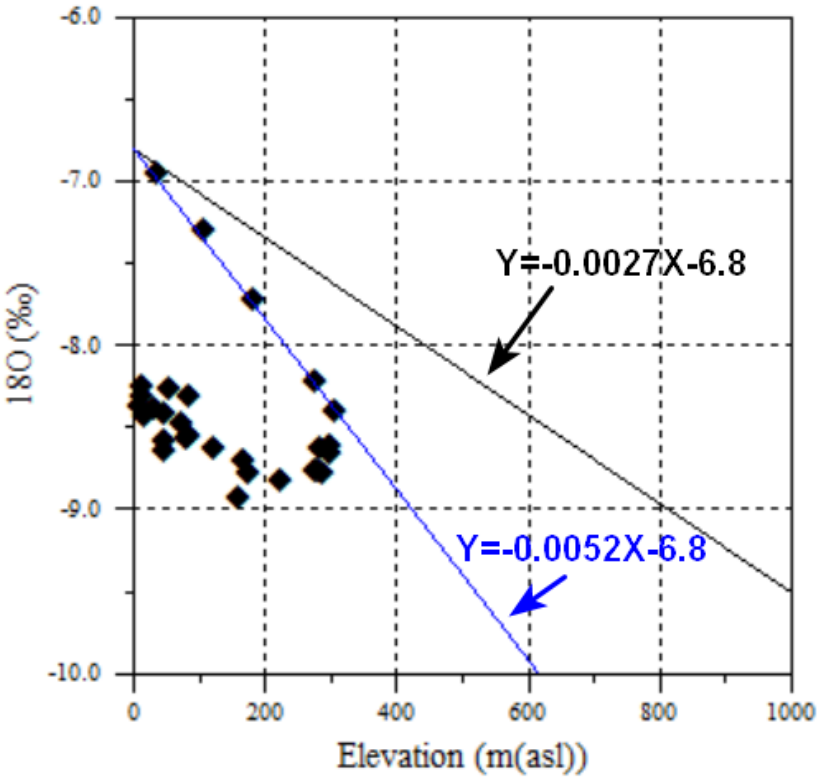

Figure 15

Altitude-$\delta^{18}O$ diagram of groundwater in the Laayoune-Dakhla region